# GYGD pore motifs in neighbouring potassium channel subunits interact to determine ion selectivity

Mark L. Chapman, Howard S. Krovetz and Antonius M. J. VanDongen

*Department of Pharmacology and Cancer Biology, Duke University Medical Center, PO Box 3813, Durham, NC 27708, USA*

(Received 11 August 2000; accepted after revision 26 September 2000)

1. Cells maintain a negative resting membrane potential through the constitutive activity of background $K^+$ channels. A novel multigene family of such $K^+$ channels has recently been identified. A unique characteristic of these $K^+$ channels is the presence of two homologous, subunit-like domains, each containing a pore-forming region. Sequence co-variations in the GYGD signature motifs of the two pore regions suggested an interaction between neighbouring pore domains.

2. Mutations of the GYGD motif in the rat drk1 (Kv2.1) $K^+$ channel showed that the tyrosine (Y) position was important for $K^+$ selectivity and single channel conductance, whereas the aspartate (D) position was a critical determinant of open state stability.

3. Tandem constructs engineered to mimic the GYGx–GxGD pattern seen in two-domain $K^+$ channels delineated a co-operative intersubunit interaction between the Y and D positions, which determined ion selectivity, conductance and gating.

4. In the bacterial KcsA $K^+$ channel crystal structure, the equivalent aspartate residue (D80) does not directly interact with permeating $K^+$ ions. However, the data presented here show that the D position is able to fine-tune ion selectivity through a functional interaction with the Y position in the neighbouring subunit.

5. These data indicate a physiological basis for the extensive sequence variation seen in the GYGD motifs of two-domain $K^+$ channels. It is suggested that a cell can precisely regulate its resting membrane potential by selectively expressing a complement of two-domain $K^+$ channels.

A fundamental physiological property of all living cells is the maintenance of a negative membrane potential. In neurons and muscle cells, the resting membrane potential controls excitability by setting the distance to the threshold for firing an action potential. In non-excitable cells, the resting membrane potential contributes to the electrochemical gradient used by pumps and transporters to move molecules into and out of the cell. Although it has been known for a long time that $K^+$-selective ion channels play a critical role in setting the resting membrane potential (Stämpfli, 1983), our understanding of the molecular nature of these channels has remained incomplete until recently. With the cloning and expression of a new class of constitutively active $K^+$ channels (Goldstein *et al.* 1996; Lesage *et al.* 1996; Fink *et al.* 1996; Duprat *et al.* 1997), it is now possible to investigate the molecular mechanisms by which the resting membrane potential is established. A unique feature of these new $K^+$ channel proteins is that they contain two homologous domains, each of which resembles an inward rectifier $K^+$ channel subunit. Each domain contains two transmembrane segments, which flank a pore-forming region with significant homology to other $K^+$-selective channels (Fig. 1).

The highly conserved pore-forming P-region has been shown to determine permeation properties in both voltage-gated and inward rectifier $K^+$ channels (Yellen *et al.* 1991; Yool & Schwarz, 1991; Hartmann *et al.* 1991; Navarro *et al.* 1996; Slesinger *et al.* 1996; Yang *et al.* 1997). In all voltage-gated $K^+$ channels and many other $K^+$-selective channels, the P-region is characterized by a signature sequence (Heginbotham *et al.* 1994), which contains the motif Gly-Tyr-Gly-Asp (GYGD). The first three residues of this motif, GYG, have been shown to contribute to the $K^+$ ion selectivity filter in the crystal structure of the bacterial KcsA $K^+$ channel (Doyle *et al.* 1998). However, the aspartate residue does not contribute to the selectivity filter and therefore does not appear to be directly involved in determining ion selectivity or permeation. The structural assignment of the selectivity filter to this portion of the protein confirmed what had previously been inferred from mutagenesis experiments, which implicated the GYG sequence as a critical determinant for $K^+$ ion selectivity and conductance (Heginbotham *et al.* 1992).

A distinguishing characteristic of the two-domain $K^+$ channels is that the GYGD motif is not strictly conserved:

a large degree of amino acid variation is seen at the Y and D positions. Therefore, these channels may not be as $K^+$ selective as their voltage-gated counterparts. This would not be surprising, since a perfectly $K^+$-selective resting conductance would drive the membrane potential to an extremely negative value, given a physiological $K^+$ ion concentration gradient, potentially making the cell unexcitable. We have tested the hypothesis that the sequence variation seen in two-domain channels affects ion selectivity and permeation properties. The results demonstrate the existence of a functional interaction between the Y position of the GYGD motif of one subunit and the D position in the neighbouring subunit. It is concluded that selectivity filter sequences of neighbouring subunits act together to fine-tune ion selectivity and regulate permeation rate and single channel gating. The data presented provide a physiological explanation for the elaborate sequence variation seen at these positions in the two-domain $K^+$ channels.

## METHODS

### Molecular biology

Mutagenesis was performed using the polymerase chain reaction (PCR) and *drk1* in the pBluescript plasmid vector. Oligonucleotides were designed using OLIGO software (National Biosciences, Inc.). Mutagenesis of small restriction fragments was performed by the 'megaprimer' technique (Sarkar & Sommer, 1990). Mutated fragments were sequenced using a 7-deaza-GTP DNA sequencing kit (Amersham). Plasmid DNA was linearized using the *Not* I restriction enzyme. Sense RNA was transcribed using T7 RNA polymerase. RNA was capped using m7G(5′)ppp(5′)G.

### Construction of dimers

Dimers were constructed using a *Sph* I restriction site located at nucleotide 1700 in the C-terminus of drk1 (Frech *et al.* 1989; amino acid 560) as previously described (Krovetz *et al.* 1997). A novel *drk1* construct was made by introducing a *Sph* I restriction site 20 nucleotides upstream of the start codon, which maintains the reading frame at nucleotide 1700 and introduces four glycine residues. Digestion of this construct with *Sph* I yielded a 1.7 kb fragment encoding amino acids 1–560. This fragment was ligated into a *drk1* construct linearized with *Sph* I to produce the tandem dimer. The ion

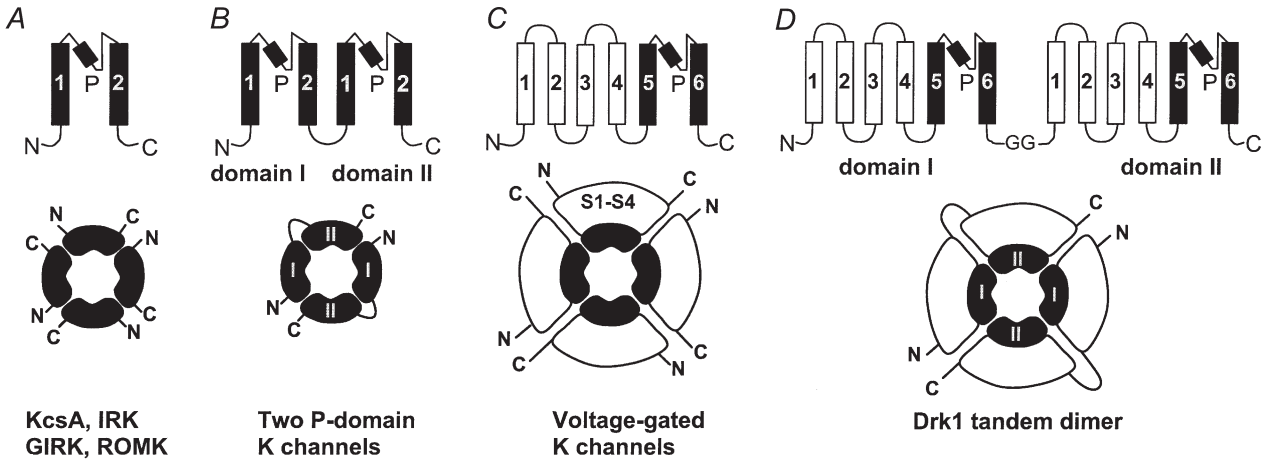


**Figure 1. Topology of $K^+$ channel families**

*A*, the topologically simplest $K^+$ channels include the strong inward rectifiers (IRK), the G-protein-gated $K^+$ channels (GIRK), the weak inward rectifiers (ROMK), as well as the recently crystallized bacterial $K^+$ channel KscA (Doyle *et al.* 1998). Their subunits contain two transmembrane segments (M1 and M2), which flank the pore-lining P-region. In the KcsA crystal structure, the P-region forms a re-entrant hairpin-loop consisting of a short alpha-helical domain (indicated by the filled rectangle), a turn and an extended structure which lines the narrow selectivity filter (Doyle *et al.* 1998). Two $K^+$ ions are seen in the selectivity filter, which are co-ordinated by the backbone carbonyl oxygens of the amino acids V, G, Y and G. Functional channels are formed by assembly of four subunits. *B*, subunits of the constitutively active two-domain $K^+$ channels contain two homologous domains which topologically resemble an inward rectifier $K^+$ channel subunit. Each domain contains two transmembrane segments, which flank a region with strong homology to other $K^+$ channel P-regions. Topologically, the two-domain $K^+$ channels therefore are equivalent to a tandem dimer of two inward rectifier $K^+$ channels. It is thought that functional channels are formed by assembly of two subunits. *C*, subunits of voltage-gated $K^+$ channels contain six transmembrane segments (S1–S6). The pore-forming P-region is localized between S5 and S6, which are similar to M1 and M2 in inward rectifier $K^+$ channels. The first four transmembrane segments (S1–S4) form the voltage sensor. Functional channels assemble from four subunits. *D*, tandem dimer constructs of the drk1 $K^+$ channel were generated for this study as described previously (Krovetz *et al.* 1997). Functional $K^+$ channels are formed by assembly of two of these dimers.

selectivity and activation properties of the wild-type–wild-type dimer were indistinguishable from those of the wild-type subunit expressed as a homotetramer.

### Electrophysiology

Oocyte preparation and cRNA injection were done as previously described (VanDongen *et al.* 1990; Wood *et al.* 1995). Briefly, oocytes were collected under 3-aminobenzoic acid ethyl ester (Tricaine) anaesthesia from adult female *Xenopus laevis* frogs that were humanely killed after the final collection. Defolliculated oocytes were placed in a recording chamber perfused with one of the following solutions (mM): $K^+$ solution: 100 KCl, 1 $MgCl_2$, 10 Hepes; $Na^+$ solution: 100 NaCl, 1 $MgCl_2$, 10 Hepes; $Cs^+$ solution: 100 CsCl, 1 $MgCl_2$, 10 Hepes; $NMDG^+$ solution: 100 NMDG-Cl, 1 $MgCl_2$, 10 Hepes. The pH was adjusted to 7.40 using KOH, NaOH, CsOH or Tris, respectively. $K^+$ currents were recorded using a commercial two-electrode voltage-clamp amplifier (Warner Instruments). Oocytes were impaled with electrodes filled with 3 M KCl. The resistances of the current and voltage electrodes were typically 0.1–0.5 MΩ. Voltage pulse protocols and data acquisition were managed by pCLAMP hardware and software (Axon Instruments). Linear leak and capacitive currents were corrected using a *P*/4 protocol. Inhibition by $Cd^{2+}$ was evaluated using step depolarizations to +40 mV from a holding potential of −80 mV. Oocytes were perfused continuously with one of the above solutions, to which $CdCl_2$ was added to obtain the desired concentration.

Single channel currents were recorded from cell-attached patches on manually devitellinized oocytes as previously described (Chapman *et al.* 1997). Patch pipettes were fabricated from thin wall borosilicate (type 7740) capillaries (TW150F, WPI, Sarasota, FL, USA), Sylgard (Dow-Corning Corp., Midland, MI, USA) coated and fire polished. Solutions were as follows (mM): bath: 100 KCl, 60 KOH, 10 EGTA, 10 Hepes and 2 $MgCl_2$, pH 7.2 with HCl; pipette: 150 NMDG-Cl, 5 KCl, 5 KOH, 2 $MgCl_2$, 2 $CaCl_2$ and 10 Hepes, pH 7.2 with HCl. Data were acquired with an Axopatch 200 patch-clamp amplifier, Digidata 1200 interface and pCLAMP 6 software (Axon Instruments). Currents were filtered at 1.5–2.5 kHz (−3 db, 4-pole Bessel filter), digitized at 5–10 kHz and stored on computer hard disk for off-line analysis. Linear leakage and capacitative currents were corrected using a smoothed average of empty traces. Single channel analysis was performed with the TRANSIT algorithm and software package (VanDongen, 1996; available for download at http://www.vandongen-lab.com).

## RESULTS

### Sequence co-variation in GYGD motifs of two-domain $K^+$ channels

With the completion of the *C. elegans* genome sequencing project, it is now possible to determine the full complement of worm genes that display sequence homology to the two-domain $K^+$ channels (Salkoff & Jegla, 1995; Wei *et al.* 1996; Bargmann, 1998). The family of two-domain $K^+$ channel genes was found to be surprisingly extensive, containing more members than all other $K^+$ channel genes found in *C. elegans* combined. When the pore-forming P-regions of these two-domain $K^+$ channels were aligned (Fig. 2), a unique sequence variation pattern was uncovered for the GYGD signature motif (Table 1). The first domain contained the sequence GYGx (where x = D, E, H, I, K, N, R, S, T or Y), while

**Table 1. GYGD sequence variation motifs in two-domain $K^+$ channels**

| Species or construct | Motif | Domain I g y g d | Domain II g y g d | No. of genes |
|---|---|---|---|---|
| *C. elegans* | 1 | y d | **F** d | 1 |
| | 2 | y d | **L** d | 1 |
| | 3 | y **E** | **F** d | 1 |
| | 4 | y **E** | **L** d | 1 |
| | 5 | y **H** | **F** d | 4 |
| | 6 | y **H** | **L** d | 2 |
| | 7 | y **I** | **F** d | 1 |
| | 8 | y **K** | **E** y d | 1 |
| | 9 | y **N** | **F** d | 7 |
| | 10 | y **N** | **L** d | 6 |
| | 11 | y **N** | y d | 2 |
| | 12 | y **R** | **L** d | 1 |
| | 13 | y **S** | **I** d | 1 |
| | 14 | y **S** | **L** d | 1 |
| | 15 | **F** **T** | **F** d | 1 |
| | 16 | y **T** | **L** d | 1 |
| | 17 | y **Y** | **F** d | 3 |
| | 18 | y **Y** | **L** d | 1 |
| *D. melanogaster* | 9 | y **N** | **F** d | 1 |
| *H. sapiens* | 6 | y **H** | **L** d | 1 |
| | 5 | y **H** | **F** d | 1 |
| | 9 | y **N** | **F** d | 2 |
| | 19 | F **N** | **F** d | 1 |
| drk1 | * | y d | y d | — |
| Y376L | * | **L** d | **L** d | — |
| D378E | * | y **E** | y **E** | — |
| Y376L + D378E | * | **L** **E** | **L** **E** | — |
| D378E–wt | * | y **E** | y d | — |
| wt–Y376L | 2 | y d | **L** d | — |
| Y376L + D378E–wt | * | **L** **E** | y d | — |
| D378E–Y376L | 4 | y **E** | **L** d | — |

Summary of the sequence variations seen at the GYGD positions in the two domains. A total of 19 different sequence variations were observed in the alignment shown in Fig. 2. Residues that deviate from the GYGD sequence are shown in bold capitals. The aspartate residue found in the second domain is absolutely conserved, along with all but one of the glycine residues. All 43 two-domain sequences show a variation of the GYGD amino acid sequence in one or both domains. Of the 43 sequences, 39 have a variation at the aspartate residue in domain I together with a variation of the tyrosine residue in domain II. The bottom section of the table summarizes GYGD motifs found in the various drk1 channel mutants and tandem constructs used in this study. Tandem dimers will be referred to in this paper by the amino acid residues found at the Y and D positions in domains I and II. For instance, the dimer in which the front half is D378E and the back half is Y376L will be referred to as 'yE-Ld'. Asterisks indicate GYGD motifs not found in the *C. elegans* genome. wt, wild-type.

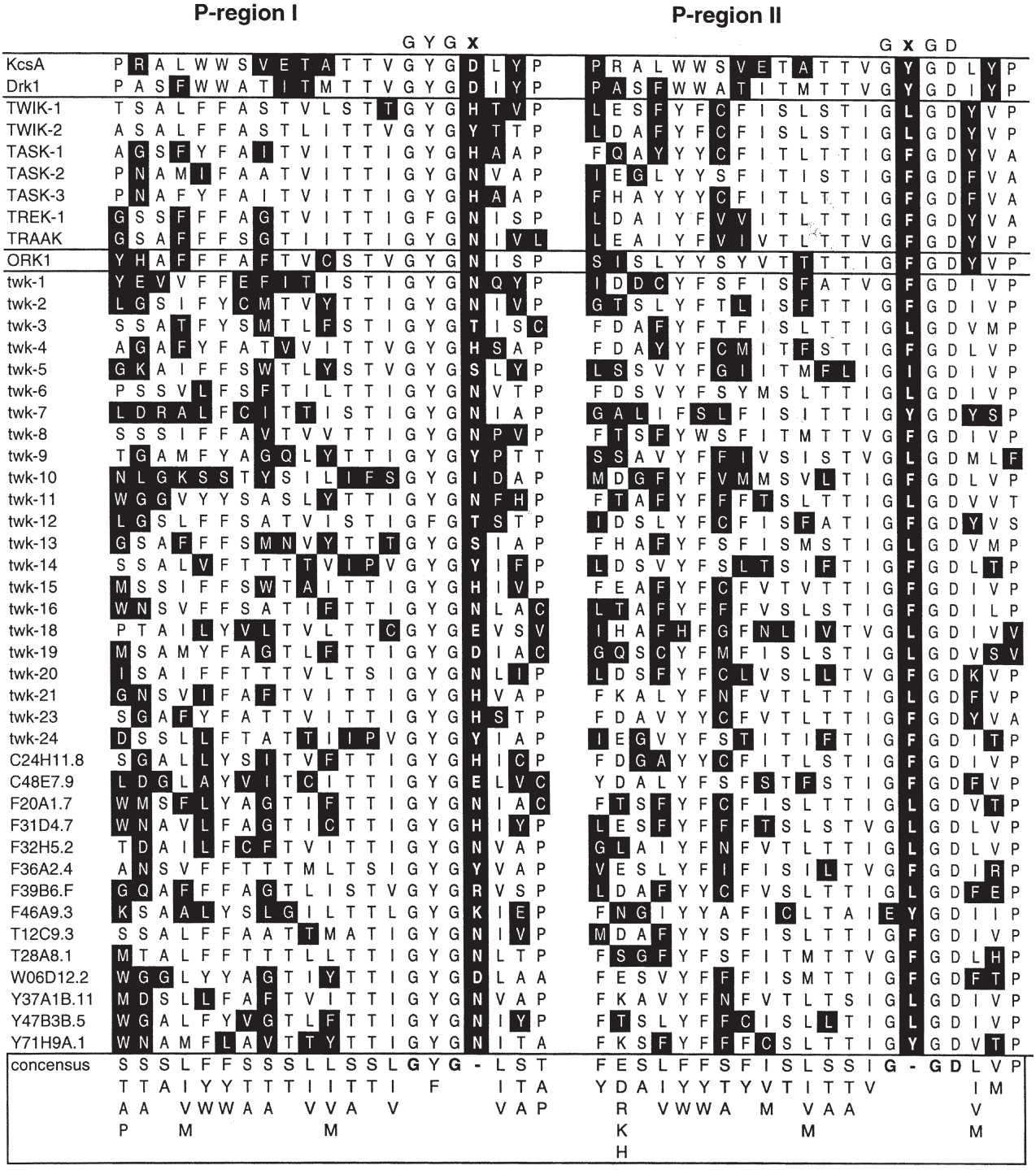


**Figure 2. Sequence conservation in P-regions of two-domain $K^+$ channels**

A BLAST search (www.ncbi.nlm.nih.gov/BLAST/) using the amino acid sequence of the human TWIK-1 $K^+$ channel identified five additional human channels (TWIK-2, TREK-1, TASK-1, TASK-2, TASK-3 and TRAAK), a *Drosophila* channel (ORK1) and 36 homologous sequences in the *C. elegans* genome. All of these sequences contain two homologous domains, each with two putative transmembrane segments which flank a conserved P-region. A sequence alignment of the two-domain channel P-regions is shown here, together with the P-regions of drk1 and KcsA. Amino acids that belong to the consensus sequence are shown on a white background, while amino acids that deviate from it are shown on a black background. The GYGD signature motif is not conserved in the two-domain $K^+$ channels. In the first domain the aspartate (D) is replaced by another amino acid (E, H, I, K, N, R, S, T or Y) in 41 of the 43 genes. In the second domain the tyrosine (Y) is replaced by another amino acid (F, I or L) in 40 of the 43 genes. In none of the sequences is GYGD present in both domains.

the second domain contained GxGD (where x = F, I, L or Y). A total of 18 unique GYGx–GxGD combinations was found in the 36 *C. elegans* genes that encode two-domain $K^+$ channels. In over 90% of the channels listed in Table 1, a GYGx sequence in domain I was combined with a GxGD motif in domain II. This highly significant co-variation suggested that the signature sequences in the two domains may functionally interact. We investigated this idea using monomeric and dimeric constructs of a voltage-gated $K^+$ channel, drk1 (Kv2.1) (Frech *et al.* 1989).

A voltage-gated $K^+$ channel was used for these studies, because it allowed us to accurately correct for leakage currents that contaminate whole-cell voltage-clamp recordings. Such a correction is not possible for voltage-independent, constitutively active channels like the two-domain $K^+$ channels. Without a proper correction for

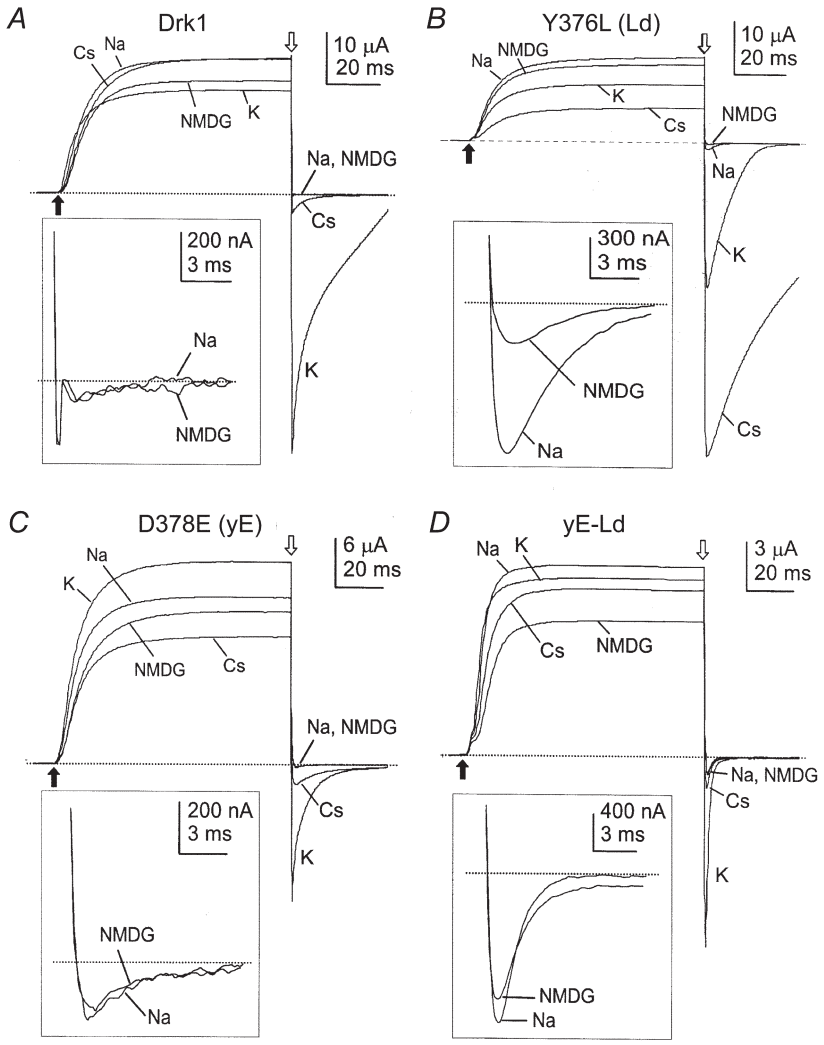


**Figure 3. $Na^+$ ion permeation and rectification in GYGD mutants**

Whole-oocyte currents are shown, which were elicited by 100 ms step depolarizations to +40 mV from a holding potential of −80 mV (indicated by the filled arrows), using a two-electrode voltage-clamp configuration. After the step depolarization the membrane potential was returned to −120 mV for 40 ms (indicated by the open arrows). Capacitive and linear leakage currents were subtracted using a *P*/4 protocol. *A*, drk1 (yd) displayed a robust, nearly ohmic $K^+$ current and a significant but small $Cs^+$ current at −120 mV. Currents recorded in $Na^+$ and $NMDG^+$ (inset) were negligibly small (less than 0.1% of the outward current) and identical in size. *B*, Y376L (Ld) remained highly permeable to $K^+$, but the current was dwarfed by that of $Cs^+$. Inward currents were noticeable in both $Na^+$ and $NMDG^+$, but $Na^+$ currents were approximately 4 times larger (inset). *C*, D378E (yE) yielded significant currents with both $K^+$ and $Cs^+$, but $K^+$ currents were strongly outwardly rectifying. As with drk1, tail currents in $Na^+$ and $NMDG^+$ were identical (inset), indicating no significant $Na^+$ permeability. *D*, the yE-Ld dimer showed pronounced inward currents in all external solutions. $K^+$ currents were also outwardly rectifying, though not as strongly as those of D378E. Tail currents for both $Na^+$ and $NMDG^+$ were large but were essentially identical in magnitude (inset).

leakage currents, subtle variations in ion selectivity cannot be experimentally determined. Because the pore-forming domains of all potassium channels are conserved, both in their membrane topology (Fig. 1) and in their amino acid sequence (Fig. 2), the results obtained here for the voltage-gated $K^+$ channel drk1 are likely to be relevant for the constitutively active two-domain $K^+$ channels.

### Mutations at the Y and D position of the GYGD motif produce distinct phenotypes

In order to examine the functional consequences of sequence variations in the GYGD motif, individual point mutations were made in the GYGD motif of the drk1 $K^+$ channel at the Y and D positions, introducing amino acids found in two-domain channels (Table 1). Since drk1 $K^+$ channels assemble as homotetramers, these mutations were present in all four subunits. At each position, only one substitution gave rise to functional channels: the tyrosine could only be mutated to a leucine without losing function, while for the aspartate, only the charge-conserving mutation to glutamate was tolerated. Each of the individual mutations Y376L (Ld) and D378E (yE) expressed robustly as homotetramers (Fig. 3). However, each mutant had a distinct phenotype. Whereas the wild-type drk1 channel (yd), like other voltage-gated $K^+$ channels, was highly selective for $K^+$ ions over $Na^+$ or $Cs^+$ ions (Fig. 3*A*), the Ld mutant preferred $Cs^+$ over $K^+$ and displayed a substantial inward $Na^+$ current (Fig. 3*B*). Mutation of Y376 therefore significantly compromised $K^+$ ion selectivity. The yE mutant, on the other hand, conducted $Cs^+$ ions poorly and was not permeable to $Na^+$

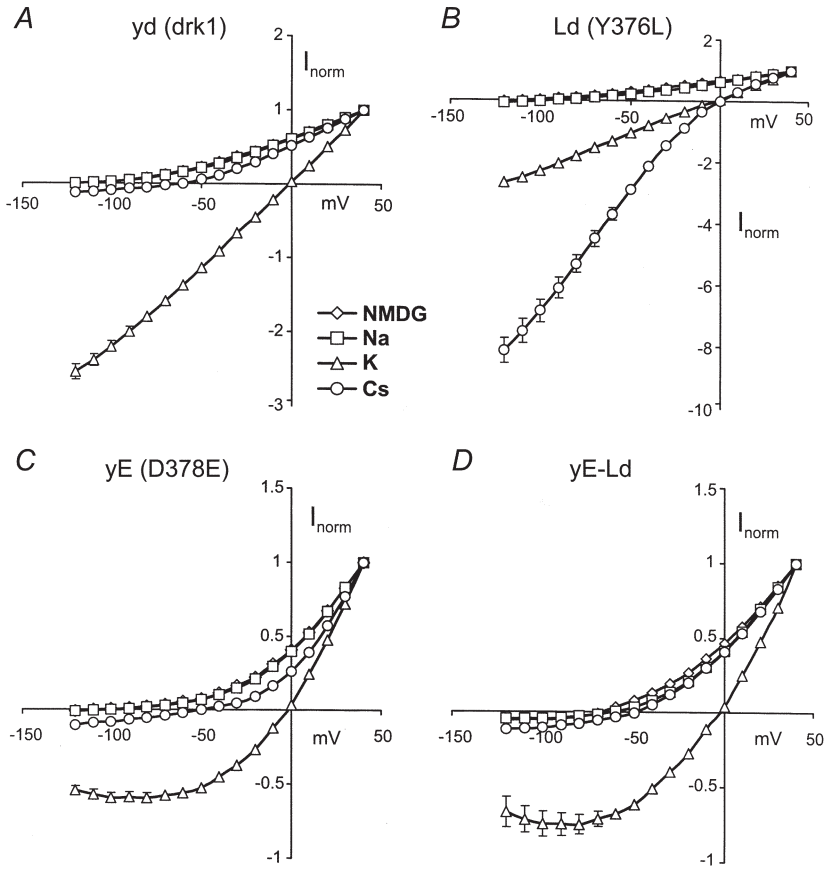


**Figure 4. Normalized *I–V* relationships in GYGD mutants**

Normalized *I–V* relationships were constructed from tail current measurements (see Figs 3 and 6). Currents were normalized by dividing by the current at +40 mV. *A*, drk1 (yd) displayed little or no inward current in either $Na^+$ or $NMDG^+$. $K^+$ currents were essentially ohmic and $Cs^+$ currents were small (~10% of outward currents) but significant. *B*, the Y376L (Ld) channel showed a small but significant $Na^+$ current, as compared to $NMDG^+$. $K^+$ currents were unaffected but $Cs^+$ currents were substantially larger than was seen for the wild-type (yd) channel. *C*, $Na^+$, $NMDG^+$ and $Cs^+$ currents were largely unaffected by the D378E (yE) mutation. $K^+$ currents, however, showed a pronounced outward rectification. *D*, combining the two mutant subunits in a tandem construct (yE-Ld) eliminated the $Na^+$ permeability introduced by the Y376L mutation. Rectification of $K^+$ currents, introduced by the D378E mutation, remained despite the mutation only being present in two of the four subunits. Most strikingly, the large increase in $Cs^+$ permeability afforded by the Y376L mutation was completely abrogated.

**Table 2. Reversal potentials of four different extracellular cations**

| | yd | yE | Ld | LE | yE-yd | yd-Ld | yd-LE | yE-Ld |
|---|---|---|---|---|---|---|---|---|
| $NMDG^+$ | −119.8 | −99.5 | −114.8 | −115.1 | −114.3 | −109.4 | −119.7 | −68.0 |
| | ± 0.9 | ± 1.6 | ± 0.8 | ± 1.3 | ± 1.1 | ± 1.4 | ± 1.3 | ± 1.6 |
| $Na^+$ | −118.3 | −96.6 | −91.7 | −95.0 | −112.1 | −98.3 | −99.6 | −64.5 |
| | ± 1.2 | ± 1.7 | ± 1.1 | ± 0.8 | ± 1.3 | ± 0.9 | ± 1.2 | ± 1.7 |
| $K^+$ | −1.9 | −2.2 | −3.3 | −3.3 | −2.9 | −2.4 | −2.5 | −3.1 |
| | ± 0.5 | ± 0.7 | ± 0.6 | ± 0.4 | ± 0.9 | ± 0.8 | ± 0.5 | ± 0.7 |
| $Cs^+$ | −59.0 | −54.3 | 0.7 | 7.9 | −56.4 | −16.4 | −16.3 | −56.0 |
| | ± 1.3 | ± 1.2 | ± 0.7 | ± 0.5 | ± 1.4 | ± 0.4 | ± 0.6 | ± 1.5 |

Reversal potentials of each of the four different extracellular cations were estimated by linear interpolation of values obtained closest to the current reversal. Values (mV) represent the mean ± S.E.M. for 8–14 observations.

ions. Like the wild-type (yd) channel, the inward current seen for yE in an all-$Na^+$ external solution was not significantly different from that seen in an external solution containing the impermeant cation $NMDG^+$ (Fig. 3*C*). Mutation of D378 therefore did not affect $K^+$ ion selectivity. However, the yE mutant displayed outward rectification, even under isotonic $K^+$ ion conditions (Figs 3*C* and 4*C*).

A consistent nomenclature will be used throughout this paper to refer to the various mutants and dimer constructs. Homomeric channels will be referred to by a two-letter code, indicating the amino acids found at the Y and D positions of the GYGD motif. Mutant residues will be in upper case, wild-type residues in lower case. For instance: Y376L = GLGD → Ld. Dimer constructs will be referred to using the codes for the parent channels separated by a hyphen. For instance the D378E–Y376L dimer will be referred to as yE-Ld.

### Effects of GYGx–GxGD sequence variations on ion selectivity

Since most two-domain $K^+$ channels contain a variant at the D position in domain I and the Y position in domain II functional channels assembled from two subunits only have two of the four Y and D positions altered. To investigate the functional consequences of such an arrangement, a dimer was constructed in which the Y376L (Ld) and D378E (yE) subunit were linked in tandem to mimic the structure of the two-domain $K^+$ channels (Fig 1*D*). The D378E–Y376L dimer (GYGE–GLGD) will be referred to from here onwards as yE-Ld to indicate the amino acid variations at the Y and D positions in the two domains (see above). The same nomenclature will be applied to other dimer constructs used in this study (as summarized in Table 1). The yE-Ld dimer retained aspects of both parent phenotypes, although each mutation was now present in only two of the four subunits. Like the monomeric Ld channel, the yE-Ld dimer showed an inward current in an all-$Na^+$ external solution. However, a nearly identical current was observed with $NMDG^+$, suggesting that most of the inward current was not an ionic current, but rather was a gating current reflecting the movement of the charged voltage sensors (Armstrong & Bezanilla, 1973). Furthermore, the ability to select against the larger $Cs^+$ ion was restored and a pronounced degree of rectification was observed (Figs 3*D* and 4*D*).

Figure 4 shows normalized instantaneous current–voltage (*I–V*) relationships constructed from data such as those shown in Fig. 3. Drk1 (yd) displayed a nearly ohmic *I–V* relationship in 100 mM external $K^+$, which is typical for the voltage-gated delayed rectifier family of $K^+$ channels. Neither $NMDG^+$ nor $Na^+$ produced an appreciable inward current. $Cs^+$ inward currents were considerably smaller than $K^+$ currents, but were still of significant magnitude (Fig 4*A*). The Y376L (Ld) mutation produced no discernible effect on $K^+$ currents at the whole-cell level, as the currents were non-rectifying and the reversal was still near 0 mV. Although inward tail currents were measurable in both $NMDG^+$ and $Na^+$, they were relatively small and not readily apparent on this scale. $Cs^+$ currents, however, were quite different from those of the wild-type channel. The reversal potential was shifted by nearly 60 mV (Table 2) and the instantaneous *I–V* curve became supra-linear indicating that $Cs^+$ was now superior to $K^+$ as a permeant ion for this channel, in terms of both permeability and conductance (Fig 4*B*). As mentioned, the D378E (yE) mutation had no effect on the ion selectivity of the channel. Consequently, *I–V* curves constructed from $NMDG^+$, $Na^+$ and $Cs^+$ data were not qualitatively different from those of drk1 (compare Fig. 4*A* with *C*). A striking difference introduced by the mutation was the pronounced degree of outward rectification now seen in the instantaneous $K^+$ current.

Combining the two point mutants in a tandem construct (yE-Ld) dramatically altered the effects of the Y376L mutation (Fig 4*D*). The tandem construct was no longer permeable to $Na^+$ ions and the preferential $Cs^+$ permeability of the Ld channel was also eliminated. Interestingly, the pronounced outward rectification observed in the homomeric yE channel was completely retained in the yE-Ld dimer, even though the D378E mutation was present in only two of the four subunits.

### A functional intersubunit interaction between the Y and D positions

Whereas Ld (Y376L) and yE (D378E) were both functional as homomeric channels, other amino acid replacements seen in two-domain channels were lethal when expressed as homomeric drk1 mutants (data not shown). We therefore chose to work with the Ld and yE channels to investigate further the possible interaction between these positions. In order to explore more fully the nature of the interaction, additional permutations of monomeric and dimeric channels were constructed and assayed for their permeability to $Na^+$, $K^+$, $Cs^+$ and $NMDG^+$ ions. Figure 5 summarizes the effects of these mutations on $K^+$ selectivity and the ability of the channels to conduct $Na^+$ and $Cs^+$ ions. As suggested by the data in Figs 3 and 4, homomeric Ld channels displayed a significant increase in $Na^+$ permeability, while both yE and the yE-Ld dimer were as $K^+$ selective as the parent channel, drk1 (yd). Although both yE and yE-Ld had pronounced inward currents in all-$Na^+$ external solutions, the same currents were present when $NMDG^+$ was substituted for $Na^+$, again indicating that the currents were not ionic and were most probably due to the return of gating charge. For this reason, the $Na^+$ permeability data were corrected for the presence of contaminating non-ionic currents by expressing them as a $Na^+/NMDG^+$ permeability ratio.

The restoration of $K^+$ selectivity in the yE-Ld dimer could be due to the reduction of the number of mutated tyrosine (Y) residues from four to two, to the replacement

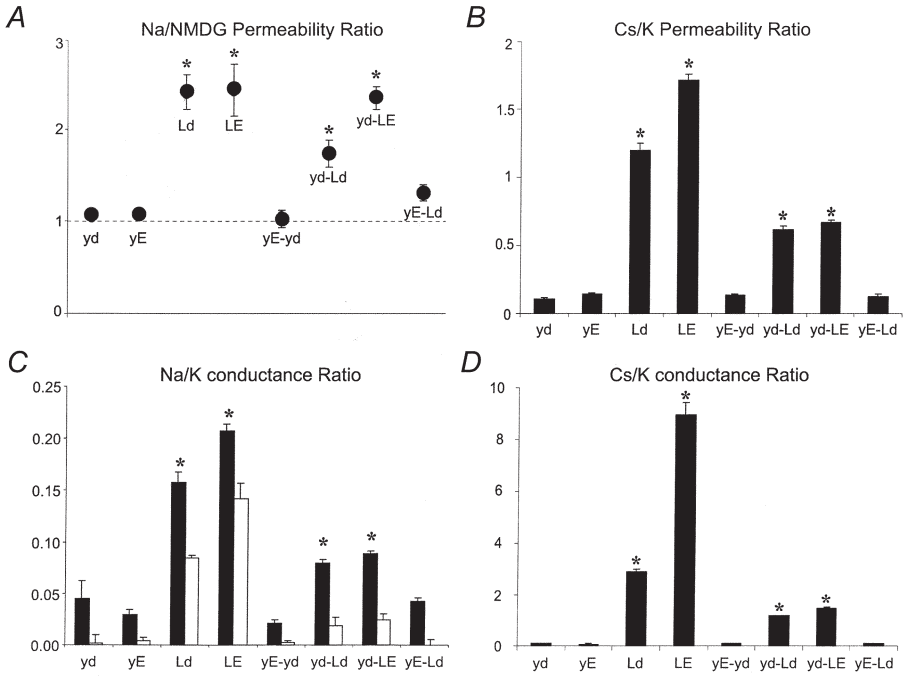


**Figure 5. Permeability and conductance ratios of GYGD mutants**

Reversal potentials were estimated by linear interpolation of values obtained closest to the current reversal. Chord conductances were calculated between the most negative membrane potential (−120 mV) and the estimated reversal potential for each oocyte. Slope conductances, where possible, were calculated between −100 and −120 mV. All conductance values were normalized for expression level by dividing them by the outward slope conductance measured between +20 and +40 mV in the same oocyte. Statistical significance was evaluated by two-way ANOVA and Dunnett's multiple comparisons (* $P < 0.01$). Values are expressed as means ± S.E.M., $n = 8$–11. The first four entries in each panel are homomeric channels. The last four entries are dimer constructs, the subunit compositions of which are found in Table 1. Permeability ratios ($P_X/P_K$) were calculated from changes in reversal potential (Hille, 1992). *A*, normalized $Na^+/NMDG^+$ permeability ratios were constructed by dividing the $Na^+/K^+$ permeability ratio by the $NMDG^+/K^+$ permeability ratio. This was necessary to correct for non-ionic components of inward currents. Therefore a value of 1 indicates no $Na^+$ permeability. All channels containing a Y376L mutation, except for yE-Ld, were permeable to $Na^+$. *B*, both Ld and LE were found to prefer $Cs^+$ over $K^+$. The yd-Ld and yd-LE dimers were less permeable to $Cs^+$ than the corresponding homomeric mutants, but still more permeable than drk1. *C*, $Na^+/K^+$ conductance ratios were constructed by dividing the $Na^+$ chord conductance by the $K^+$ slope conductance measured between −100 and −120 mV (■). The same data were replotted after correcting for non-ionic components of the current (□). *D*, $Cs^+/K^+$ conductance ratios were calculated by dividing $Cs^+$ slope conductances by $K^+$ slope conductances.

of the aspartate residue (D) with glutamate (E), or to a combination of the two. This was further investigated using additional mutants and dimer constructs. In contrast to the yE-Ld dimer, introducing both mutations in a single subunit (Y376L + D378E or LE) failed to restore ion selectivity. The homomeric double mutant LE had a phenotype similar to that of the homomeric Ld. Introducing a glutamate at the aspartate position therefore is not sufficient to restore $K^+$ selectivity. As expected, pairing a $K^+$-selective D378E (yE) subunit with a wild-type drk1 (yd) subunit (to yield the tandem yE-yd) did not diminish selectivity. The wild-type–Y376L dimer (yd-Ld), however, was superior to the homomeric Ld channel in its ability to discriminate against $Na^+$. This increase in ion selectivity was not sufficient to restore normal function to the channel, however, as the $Na^+$ permeability was still significantly greater than that seen in drk1 (yd).

Similar changes in permeability were observed with the larger $Cs^+$ ion, but the effects were much more pronounced. Drk1 (yd) displayed a $Cs^+/K^+$ permeability ratio of approximately 0.1 and was indistinguishable from yE, yE-yd and yE-Ld. In contrast, the Ld and LE homomeric channels had permeability ratios of 1.2 and 1.7, respectively, indicating that these channels preferred $Cs^+$ over $K^+$. Expressing the Ld and LE subunits in tandem with a drk1 subunit (yd-Ld and yd-LE, respectively) partially reversed the loss of $K^+$ selectivity, but still left the channels significantly permeable to $Cs^+$. Conductances of $Na^+$ (Fig. 5*C*) and $Cs^+$ (Fig. 5*D*) were reflective of their permeabilities. Again, all channels possessing the Y376L mutation, except for the yE-Ld dimer, showed significantly increased $Cs^+$ and $Na^+$ conductances compared to wild-type drk1. As with the permeability, the differences were more pronounced with $Cs^+$ than with $Na^+$, as the Ld and LE channels showed 30-fold and 100-fold increases in $Cs^+$ conductance, respectively, *versus* the wild-type (yd) channel.

Taken together, the data shown in Fig. 5 demonstrate the presence of an intersubunit functional interaction between the Y and D positions of the selectivity filter. Introduction of the Y376L mutation in the drk1 channel resulted in a severe decrement of $K^+$ selectivity and enhanced $Cs^+$ conductance. Restoration of wild-type permeation properties required that: (i) the number of Y376L subunits per channel was reduced from four to two, (ii) two subunits contained the mutation D378E (compare yd-Ld and yE-Ld), and (iii) the Y376L and D378E mutations were present in neighbouring subunits (compare yd-LE and yE-Ld). Introduction of the D378E mutation into the neighbouring pore sequence was both necessary and sufficient to restore selectivity to the Y376L channel. Accordingly, the Y376L channel could not be 'rescued' by tandem expression with a wild-type subunit.

The importance of this finding is underscored by the occurrence of this particular pore motif (yd-Ld) within the family of two-domain $K^+$ channels (see Table 1). Recordings of this channel with $NMDG^+$ as the extracellular cation showed normal activation and permeability to $K^+$ (Fig. 6*A*). Substitution of NaCl for

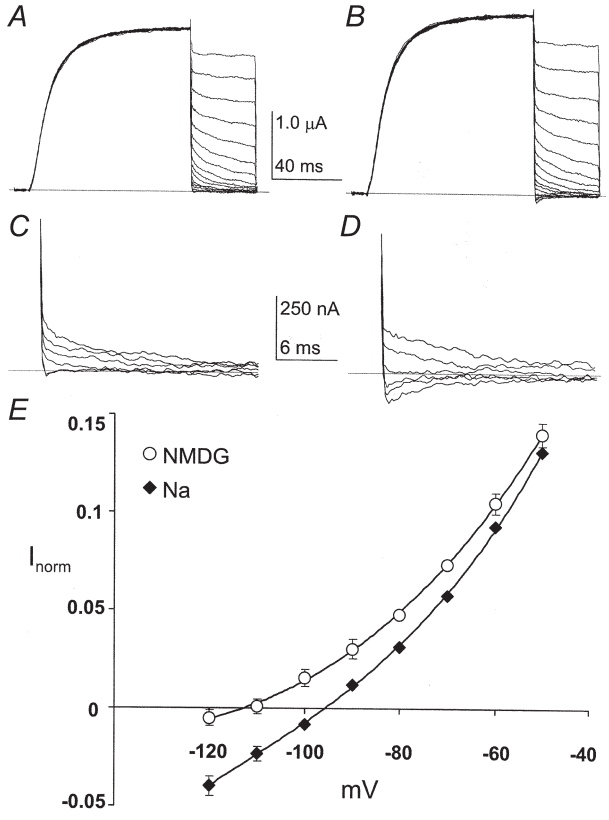


**Figure 6. $Na^+$ permeability of the wild-type–Y376L (yd-Ld) tandem channel**

Families of whole-oocyte currents are shown for the yd-Ld tandem channel. The tandem pore motif of this channel (gygd–gLgd) is found in the twk-19 two-domain $K^+$ channel of *C. elegans*. Currents were elicited by 100 ms step depolarizations to +40 mV from a holding potential of −80 mV. After the step depolarization the membrane potential was returned to tail potentials from +30 to −120 mV in 10 mV increments for 40 ms. Capacitive and linear leakage currents were subtracted using a *P*/4 protocol. *A*, a family of currents recorded with 100 mM $NMDG^+$ as the external cation. *B*, the same oocyte as in *A* with 100 mM $Na^+$ as the external cation. *C*, an expanded view of the $NMDG^+$ tail currents (from −80 to −120 mV) from *A*. *D*, an expanded view of the $Na^+$ tail currents from *B*. *E*, normalized *I–V* relationships for the yd-Ld tandem channel. Currents were normalized to the current at +40 mV.

NMDG-Cl in the external solution revealed small but significant inward $Na^+$ currents (Fig. 6*B*). Comparison of the currents near the reversal potentials shows that the currents recorded in $NMDG^+$ were nearly identical at −120 and −110 mV (Fig. 6*C*). Such saturation is to be expected of gating currents but generally would not be seen in ionic currents. In contrast, the inward $Na^+$ currents were larger and did not saturate (Fig. 6*D*) indicating that they arose from $Na^+$ influx. The differences are better appreciated in the normalized *I–V* relationship shown in Fig. 6*E*. The currents were indistinguishable at a potential of −50 mV but began to diverge at more negative potentials. Sodium currents reversed at potentials nearly 10 mV more negative and the inward currents were substantially larger than the corresponding $NMDG^+$ currents. Both of these observations indicate that the yd-Ld channel is significantly permeable to $Na^+$.

### Single channel characteristics of GYGD mutants

Two of the common functional characteristics of two-domain $K^+$ channels are outward rectification and brief, flickery openings (Gray *et al.* 1998; Goldstein *et al.* 1998; Kim *et al.* 1998). Mutation of the aspartate of the GYGD sequence led to a marked outward rectification of whole-cell currents, even with approximately isotonic $K^+$ concentrations (see Figs 3*C* and *D*, and 4*C* and *D*). Determination of the effects of these mutations on open–closed behaviour can only be accomplished at the single channel level. Figure 7 shows representative single channel records for drk1 (yd), D378E (yE) and the yE-Ld dimer. The Y376L (Ld) mutation, in addition to substantially decreasing ion selectivity, also decreased the permeation rate to an unresolvable level. Therefore, non-stationary fluctuation analysis was used to estimate the single channel conductance (Neher & Stevens, 1977; Sigworth, 1980; Chung & Pulford, 1993). An example of a mean current–variance plot is shown in Fig. 7*B*. Whereas the Y376L (Ld) mutation produced a significant reduction in single channel conductance, the D378E (yE) mutation had no significant effect on permeation rate but markedly reduced open time and open probability.

As previously seen for whole-cell conductance and selectivity, combining these mutant subunits in the yE-Ld dimer restored the drastically lowered single channel conductance seen in the homomeric Ld channel. Interestingly, the single channel behaviour of the yE-Ld dimer, while resembling that of drk1 at the whole-cell level, was more like that of yE. These results are summarized in Fig. 8 and Table 3. Figure 8*A* shows the single channel current–voltage relationships for drk1 (yd), D378E (yE), Y376L (Ld) and the yE-Ld dimer. The Ld channel displayed a greater than 20-fold reduction in single channel conductance compared to drk1 (0.47 *versus* 10.6 pS, respectively). In contrast, the conductance of the yE channel was reduced by only 32%. When these subunits were combined in yE-Ld, the conductance was quite similar to that of the yE homomeric channel and showed less than a 50% decrease from that of drk1 (yd).

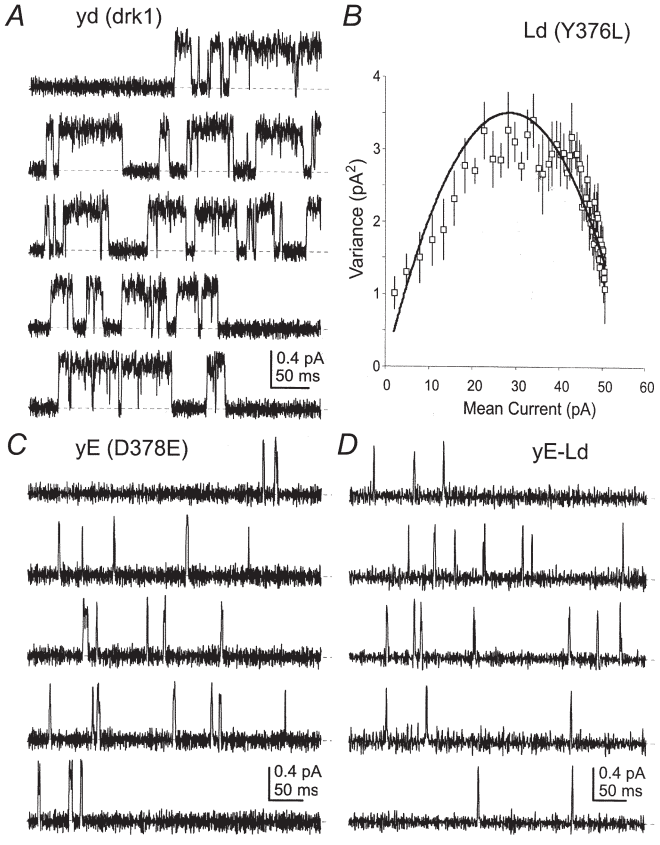


**Figure 7. Representative single channel recordings and noise analysis**

*A*, drk1 single channel traces recorded from cell-attached patches. Dashed lines indicate the zero current (closed) level. *B*, mean–variance plot calculated from multi-channel patch-clamp records of Y376L. Because discrete openings were too small to be resolved, fluctuation analysis was used to determine conductance and open probability. Symbols and bars represent the mean ± S.E.M. of 20 binned current values from 88 episodes of 30 ms at +40 mV. The continuous line is a fit of the function $s^2 = iI - I^2/N$ (Sigworth, 1980), where $s$ is the variance, $i$ is the single channel current, $I$ is the macroscopic current and $N$ is the number of channels. *C*, the behaviour of D378E was markedly different from drk1. Open time and open probability were dramatically decreased, while current amplitude was largely unaffected. *D*, the yE-Ld dimer was remarkably similar to D378E in open time, open probability and single channel current.

Very similar results were obtained from comparisons of single channel open time distributions (Fig 8*B*). The open time distribution of yE-Ld was mono-exponential with a mean of 0.83 ms, quite similar to the open time of yE, but more than 15-fold less than that of drk1 (yd). Direct measurement of the open time of Ld was not possible, because currents through individual channels could not be resolved. However, inferences can be made based upon the open probability estimated from the mean–variance analysis (Fig. 7*B* and Table 3). At a potential of 0 mV, Ld was open approximately 50% of the time, in close agreement with the open probability of drk1 (yd). The simplest interpretation of this similarity in open probability is that the mean open and closed times of the Ld channel were not much affected by the Y376L mutation. This sharply contrasts with yE and yE-Ld, both of which showed reductions of approximately 10-fold in open time and 20-fold in open probability.

**Table 3. Single channel properties**

| Construct | Conductance (pS) | Open time (ms) | $P_{open}$ |
|---|---|---|---|
| Drk1 | 10.6 ± 0.4 | 13.1 ± 0.4 | 47.5 ± 2.6 |
| D378E | 7.2 ± 0.1 | 1.47 ± 0.05 | 2.6 ± 0.4 |
| Y376L | 0.47 ± 0.03 | n.d. | 54 |
| yE-Ld | 5.4 ± 0.1 | 0.83 ± 0.01 | 2.3 ± 0.2 |

Values were derived from data such as those shown in Figs 3 and 4. Idealization of single channel activity and statistical analysis were performed with the TRANSIT software package (VanDongen, 1996). Conductance values represent slope conductances between 0 and +40 mV or 0 and +60 mV ($n = 3$–5, mean ± S.E.M.). Mean open times were determined from data at 0 mV ($n = 3$–5, mean ± S.E.M.; n.d., unable to determine, see text). Open probabilities ($P_{open}$) were determined from data at 0 mV ($n = 1$–5, mean ± S.E.M.). Open probabilities at +40 mV for drk1 and Y376L were 69 ± 5% ($n = 4$) and 75 ± 5% ($n = 7$), respectively.

## DISCUSSION

The combination of point mutations in two neighbouring GYGD motifs, shown here for the drk1 $K^+$ channel, revealed a functional interaction between selectivity filter sequences of neighbouring $K^+$ channel subunits. The presence of such an interaction was suggested by the complementary pattern of sequence variation seen in two-domain $K^+$ channels. The interaction was shown to be a critical determinant of both gating and permeation properties and suggests that the pattern of sequence variation seen in two-domain channels is of physiological significance.

It is not surprising that intersubunit interactions exist in $K^+$ channels, given the close packing of the subunits and the co-operative nature of single channel gating. However, the assignment of the interacting residues to the Y and D positions of the GYGD motif, as well as the functional consequences of this interaction, are somewhat unexpected in the light of the recently published crystallographic structure of the bacterial KcsA $K^+$ channel (Doyle *et al.* 1998). The residue analogous to D378 in KcsA, D80, does not contribute to the selectivity filter. Consistent with this structural assignment, mutating D378 in drk1 by itself had little or no effect on single channel conductance or ion selectivity. Conversely, the backbone carbonyl oxygen of Y78 in KcsA is directly involved in co-ordination of the permeant $K^+$ ions (Doyle *et al.* 1998). This explains why mutation of the

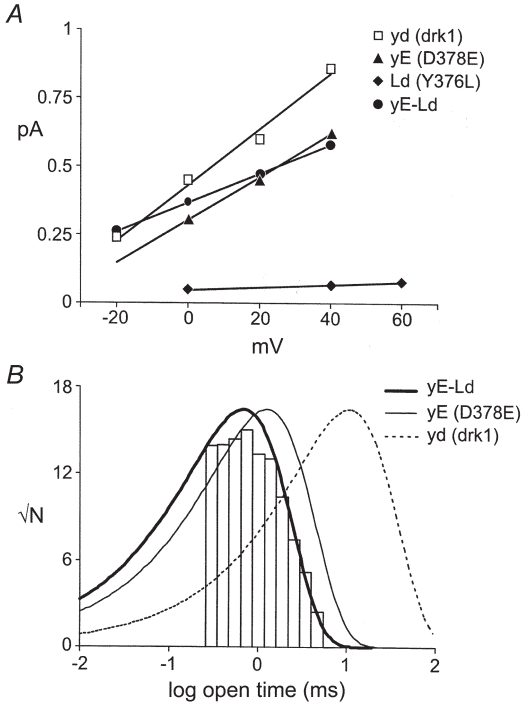


**Figure 8. Single channel conductance and open time distributions**

*A*, the single channel conductance of Y376L was reduced more than 20-fold *versus* drk1 while D378E and yE-Ld were reduced by less than 50%. Continuous lines represent linear regressions through the data points. Error bars, where applicable, have been omitted for clarity. *B*, the open time distribution of yE-Ld was mono-exponential and the mean open time was approximately 15-fold shorter than that of drk1. Thin continuous and dashed lines represent single exponential fits of open time distributions for D378E and drk1, respectively.

corresponding tyrosine (Y376) in drk1 had pronounced effects on both permeation rate and ion selectivity.

What cannot be predicted from the structure, however, is the presence of an intersubunit interaction between these positions. Analysis of the KcsA structure shows the alpha-carbons of these interacting residues to be approximately 8 Å apart. Such a distance only allows a direct physical interaction between the two residues when their side-chains are optimally positioned, which is not the case in the KscA structure. Physical interaction therefore would require either rotation of one or both side-chains, or a movement of the peptide backbone. It must be noted, however, that the atomic co-ordinates provided by the crystal structure represent only one conformation of the channel. Since the KcsA crystal was obtained at neutral pH, where the open probability of the channel is very low, the structure possibly represents a snapshot of the closed state (Clapham, 1999). Therefore it is conceivable that activation-induced changes in the structure of the selectivity filter may allow for direct physical interaction of these residues when the channel is open. Spin-labelling experiments designed to measure gating-induced structural changes in KcsA have recorded significant rearrangements of the second transmembrane segment upon activation (Perozo *et al.* 1998). However, these same techniques have failed to note any significant movement of the external vestibule, which is directly adjacent to the selectivity filter (Perozo *et al.* 1999). Given these findings, it seems unlikely that the observed functional interaction results from a direct physical interaction between these two residues. It is more likely that the Y–D interaction is due to a propagative steric effect. Mutation of the bulky tyrosine residue to the smaller leucine alters the interaction of its side-chain with its local environment. This disruption of side-chain interactions then requires a subsequent change of the neighbouring aspartate residue (in this case to the larger glutamate) to offset the effect, suggesting that the interaction proceeds through an unidentified intervening entity (Horovitz & Fersht, 1990; Horovitz, 1996).

Regardless of the precise molecular interactions, it appears that eukaryotic organisms have taken advantage of the consequences of the Y–D interaction in generating a diverse gene family which is well suited for controlling membrane potential. The combined effect of point mutations in two neighbouring GYGD motifs offers an explanation for the unique sequence co-variation seen in GYGD motifs of two-domain $K^+$ channels. It is likely that the presence of a L or F residue at the Y position in one of the domains has evolved to relax the stringent $K^+$ selectivity seen in voltage-gated $K^+$ channels. This alteration must be coupled with a subsequent change at the D position of the neighbouring subunit to achieve the proper end result of a moderate reduction of $K^+$ selectivity, maintenance of single channel conductance, low open probability, outward rectification of currents and exclusion of larger monovalent cations. These attributes will limit membrane hyperpolarization, protect the cell from becoming unexcitable and eliminate the possibility of blockade by or accumulation of potentially toxic large monovalent cations while, at the same time, preventing the two-domain channels from acting as a voltage clamp, such as might occur if the open probability was high and there was no rectification of the current.

While there was not a significant increase in $Na^+$ permeability in the yE-Ld dimer channel, there were other attributes suitable for background $K^+$ channels. Most notable of these attributes were outward rectification and a low open probability. Furthermore, the yd-Ld channel, whose pore motif combination is represented in the *C. elegans* genome (motif no. 2 in Table 1), did show a significant reduction in $K^+$ selectivity. Therefore, it is probable that other combinations of amino acids would have different effects on the $Na^+/K^+$ selectivity ratio. If the two-domain channels are instrumental in determining the resting membrane potential, it would be necessary to have many different channels with slightly varied selectivities to achieve a wide range of resting potentials. Presently there are almost 40 genes encoding two-domain channels in *C. elegans*. The sequences within this family display a repertoire of 18 unique pairs of amino acids at the Y and D positions. Tissue-specific expression for four of these two-pore domain channels was characterized in *C. elegans*, using green fluorescent protein reporters linked to gene-specific promoters (Salkoff *et al.* 1999). The four genes investigated showed tissue-specific, non-overlapping expression in both neuronal and non-neuronal cells. These data, when combined with the results of our studies, lead to the intriguing possibility that cells can precisely control their resting membrane potential and rectification properties by selectively expressing a single member of this large family of constitutively active channels.

Armstrong, C. M. & Bezanilla, F. (1973). Currents related to movement of gating particles of the sodium channels. *Nature* **242**, 459–461.

Bargmann, C. I. (1998). Neurobiology of the *Caenorhabditis elegans* genome. *Science* **282**, 2028–2033.

Chapman, M. L., VanDongen, H. M. A. & VanDongen, A. M. J. (1997). Activation-dependent subconductance levels in K channels suggest a subunit basis for ion permeation and gating. *Biophysical Journal* **72**, 708–719.

Chung, S.-H. & Pulford, G. (1993). Fluctuation analysis of patch-clamp or whole-cell recordings containing many single channels. *Journal of Neuroscience Methods* **50**, 369–384.

Clapham, D. E. (1999). Unlocking family secrets: $K^+$ channel transmembrane domains. *Cell* **97**, 547–550.

Doyle, D. A., Cabral, J. M., Pfuetzner, R. A., Kuo, A., Gulbis, J. M., Cohen, S. L., Chait, B. T. & Mackinnon, R. (1998). The structure of the potassium channel: molecular basis of K conduction and selectivity. *Science* **280**, 69–76.

Duprat, F., Lesage, F., Fink, M., Reyes, R., Heurteaux, C. & Lazdunski, M. (1997). TASK, a human background $K^+$ channel to sense external pH variations near physiological pH. *EMBO Journal* **16**, 5464–5471.

Fink, M., Duprat, F., Lesage, F., Reyes, R., Romey, G., Heurteaux, C. & Lazdunski, M. (1996). Cloning, functional expression and brain localization of a novel unconventional outward rectifier $K^+$ channel. *EMBO Journal* **15**, 6854–6862.

Frech, G. C., VanDongen, A. M. J., Schuster, G., Brown, A. M. & Joho, R. H. (1989). A novel potassium channel with delayed rectifier properties isolated from rat brain by expression cloning. *Nature* **340**, 642–645.

Goldstein, S. A., Price, L. A., Rosenthal, D. N. & Pausch, M. H. (1996). ORK1, a potassium-selective leak channel with two pore domains cloned from *Drosophila melanogaster* by expression in *Saccharomyces cerevisiae*. *Proceedings of the National Academy of Sciences of the USA* **93**, 13256–13261.

Goldstein, S. A., Wang, K. W., Ilan, N. & Pausch, M. H. (1998). Sequence and function of the two P domain potassium channels: implications of an emerging superfamily. *Journal of Molecular Medicine* **76**, 13–20.

Gray, A. T., Winegar, B. D., Leonoudakis, D. J., Forsayeth, J. R. & Yost, C. S. (1998). TOK1 is a volatile anesthetic stimulated $K^+$ channel. *Anesthesiology* **88**, 1076–1084.

Hartmann, H. A., Kirsch, G. E., Drewe, J. A., Taglialatela, M., Joho, R. H. & Brown, A. M. (1991). Exchange of conduction pathways between two related potassium channels. *Science* **251**, 942–944.

Heginbotham, L., Abramson, T. & Mackinnon, R. (1992). A functional connection between pores of distantly related ion channels as revealed by mutant $K^+$ channels. *Science* **258**, 1152–1155.

Heginbotham, L., Lu, Z., Abramson, T. & Mackinnon, R. (1994). Mutations in the K channel signature sequence. *Biophysical Journal* **66**, 1061–1067.

Hille, B. (1992). *Ionic Channels of Excitable Membranes*. Sinauer Associates Inc., Sunderland, MA, USA.

Horovitz, A. (1996). Double-mutant cycles: a powerful tool for analyzing protein structure and function. *Folding and Design* **1**, R121–126.

Horovitz, A. & Fersht, A. R. (1990). Strategy for analysing the co-operativity of intramolecular interactions in peptides and proteins. *Journal of Molecular Biology* **214**, 613–617.

Kim, D., Fujita, A., Horio, Y. & Kurachi, Y. (1998). Cloning and functional expression of a novel cardiac two-pore background $K^+$ channel (cTBAK-1). *Circulation Research* **82**, 513–518.

Krovetz, H. S., VanDongen, H. M. A. & VanDongen, A. M. J. (1997). Atomic distance estimates from novel disulfide bonds and high-affinity metal binding sites support a radial model for the K channel pore. *Biophysical Journal* **72**, 117–126.

Lesage, F., Guillemare, E., Fink, M., Duprat, F., Lazdunski, M., Romey, G. & Barhanin, J. (1996). TWIK-1, a ubiquitous human weakly inward rectifying K channel with a novel structure. *EMBO Journal* **15**, 1004–1011.

Navarro, B., Kennedy, M. E., Velimirovic, B., Bhat, D., Peterson, A. S. & Clapham, D. E. (1996). Nonselective and Gbeta-gamma-insensitive weaver K channels. *Science* **272**, 1950–1953.

Neher, E. & Stevens, C. F. (1977). Conductance fluctuations and ionic pores in membranes. *Annual Review of Biophysics and Bioengineering* **6**, 345–381.

Perozo, E., Cortes, D. M. & Cuello, L. G. (1998). Three-dimensional architecture and gating mechanism of a $K^+$ channel studied by EPR spectroscopy. *Nature Structural Biology* **5**, 459–469.

Perozo, E., Cortes, D. M. & Cuello, L. G. (1999). Structural rearrangements underlying $K^+$-channel activation gating. *Science* **285**, 73–78.

Salkoff, L. & Jegla, T. (1995). Surfing the DNA databases for $K^+$ channels nets yet more diversity. *Neuron* **15**, 489–492.

Salkoff, L., Kunkel, M. T., Wang, Z.-W., Butler, A., Yuan, A., Nonet, M. & Wei, A. (1999). The impact of the *Caenorhabditis elegans* genome project on potassium channel biology. In *Current Topics in Membranes*, vol. 46, ed. Kurachi, Y., Jan, L. Y. & Lazdunski, M., pp. 9–28. Academic Press, San Diego.

Sarkar, G. & Sommer, S. S. (1990). The "megaprimer" method of site-directed mutagenesis. *Biotechniques* **8**, 404–407.

Sigworth, F. J. (1980). The conductance of sodium channels under conditions of reduced current at the node of Ranvier. *Journal of Physiology* **307**, 131–142.

Slesinger, P. A., Patil, N., Liao, Y. J., Jan, Y. N., Jan, L. Y. & Cox, D. R. (1996). Functional effects of the mouse weaver mutation of G protein-gated inwardly rectifying $K^+$ channels. *Neuron* **16**, 321–331.

Stämpfli, R. (1983). Electrophysiology and morphology of myelinated nerve fibers. *Experientia* **39**, 931–935.

VanDongen, A. M. J. (1996). A new algorithm for idealizing single ion channel data containing multiple unknown conductance levels. *Biophysical Journal* **70**, 1303–1315.

VanDongen, A. M. J., Frech, G. C., Drewe, J. A., Joho, R. H. & Brown, A. M. (1990). Alteration and restoration of $K^+$ channel function by deletions at the N- and C-termini. *Neuron* **5**, 433–443.

Wei, A., Jegla, T. & Salkoff, L. (1996). Eight potassium channel families revealed by the *C. elegans* genome project. *Neuropharmacology* **35**, 805–829.

Wood, M. W., VanDongen, H. M. A. & VanDongen, A. M. J. (1995). Structural conservation of ion conduction pathways in K channels and glutamate receptors. *Proceedings of the National Academy of Sciences of the USA* **92**, 4882–4886.

Yang, J., Yu, M., Jan, Y. N. & Jan, L. Y. (1997). Stabilization of ion selectivity filter by pore loop ion pairs in an inwardly rectifying potassium channel. *Proceedings of the National Academy of Sciences of the USA* **94**, 1568–1572.

Yellen, G., Jurman, M. E., Abramson, T. & Mackinnon, R. (1991). Mutations affecting internal TEA blockade identify the probable pore-forming region of a K channel. *Science* **251**, 939–942.

Yool, A. J. & Schwarz, T. L. (1991). Alteration of ionic selectivity of a K channel by mutation of the H5 region. *Nature* **349**, 700–704.

**Acknowledgements**

We would like to thank Richard Whorton and John York for helpful discussions. This work was supported by grant NS31557 from the National Institute of Neurological Disorders and Stroke to A.M.J.V.D.

**Corresponding author**

A. M. J. VanDongen: Department of Pharmacology and Cancer Biology, Duke University Medical Center, PO Box 3813, Durham, NC 27708, USA.

Email: vando005@mc.duke.edu